Instabilities in a compressible hyperelastic cylindrical channel under internal pressure and external constraints

Sumit Mehta [a], Gangadharan Raju [a], S. Kumar [b], Prashant Saxena [b],*

[a] *Department of Mechanical and Aerospace Engineering, Indian Institute of Technology Hyderabad, India*
[b] *James Watt School of Engineering, University of Glasgow, Glasgow G12 8LT, UK*

ARTICLE INFO

ABSTRACT

Pressurised cylindrical channels made of soft materials are ubiquitous in biological systems, soft robotics and metamaterial designs. In this paper, we study large deformation and subsequent instability of a thick-walled and compressible hyperelastic cylinder under internal pressure and external constraints. The applied pressure can lead to elastic bifurcations along the axial or circumferential direction. Perturbation theory is used to derive the partial differential equations that govern the bifurcation behaviour of the cylindrical channel. Two cases of boundary conditions on the outer surface of the cylinder, namely, free and constrained are studied to understand their influence on the instability behaviour. The derived equations are solved numerically using the compound matrix method to evaluate the critical pressure for instability. The effects of the wall-thickness of the cylinder and the compressibility of the material on the critical pressure is investigated for both the boundary conditions. The results reveal that for an isotropic material, the bifurcation occurs along the axial direction of the cylinder at lower critical pressure compared to circumferential direction for all cases considered herein. Finally, the tuneability of the bifurcation behaviour of transversely isotropic cylinder is demonstrated by considering reinforcements along the cylinder's axis, triggering bifurcation in the circumferential direction in certain cases. The findings of the study indicate that the instability-induced pattern formation will be useful for designing shape changing material systems such as soft robotics and soft metamaterials.

1. Introduction

Soft materials such as gels, soft tissues, and elastomers can undergo large deformation that can trigger elastic instabilities such as wrinkling and folding resulting in pattern formation [1,2]. The advantage of such materials is that they have high strength to modulus ratio and therefore can sustain large strain. Typically, they possess low elastic modulus which makes them prone to elastic instabilities such as wrinkling, creasing, and folding. A cylindrical channel made of soft hyperelastic material can undergo large deformation due to inflating pressure and can exhibit wrinkle patterns either along the circumferential or axial direction as shown in Fig. 1. These undulating surface topographies are widely observed in biological systems such as skin, intestine, and mucus airways [3]. Bifurcation of thin incompressible cylinder under inflating pressure is an extensively studied problem [4–6] in literature. Bifurcation analysis of compressible hyperelastic cylindrical structure [7–9], and bilayer structures [10,11] under axial compression has also been conducted. Eversion of both compressible and incompressible elastic cylinder was studied by Chen and Haughton [12] and Haughton and Chen [13]. However, there is a lack of a detailed bifurcation analysis of a pressurised compressible thick-walled

cylinder. Thin-walled elastic tubes may experience bulging and bending depending upon their length. On the contrary, a thick cylinder tends to deform homogeneously, then bifurcates and undulates either along the axial or the circumferential direction. By constraining the external lateral boundary and the axial stretch to unity, we study the circumferential and axial bifurcation phenomena in a pressurised compressible hyperelastic cylindrical channel as shown in Fig. 1. This avoids the possibility of localised bulging as studied by Kyriakides and Yu-Chung [14] and Fu et al. [15]. In their experimental work, Cheewaruangroj et al. [16] also showed the formation of peristaltic modulation i.e., an alternation of contraction and expansion of the cylinder radius. Furthermore, we limit our discussion to only wrinkling instabilities and have not considered creasing [17,18], and folding [19,20] phenomena which are also possible in soft solids.

Pressurised soft thick cylindrical channels are common surrogates to study biological systems such as blood flow through arteries [21], soft tissue deformation [22], and have many clinical application such as biocompatible chips (organs on chips) and medical implants [23,24]. Beyond these biomedical applications, soft channels also have important application in metamaterials used for developing soft robotics [25]
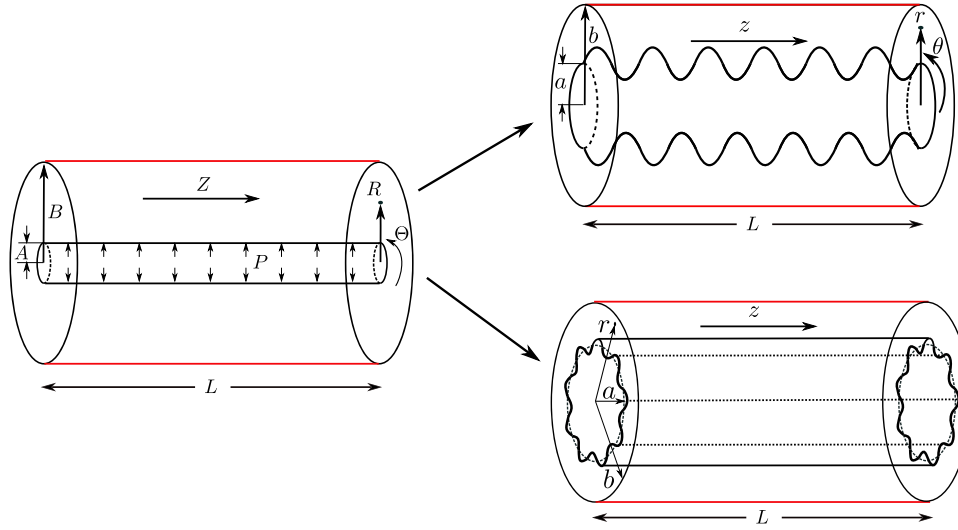

Fig. 1. A long thick compressible cylindrical tube with internal radius A, external radius B and length L in the reference configuration that deforms to a cylinder with internal radius a and external radius b under an internal pressure and plane strain condition. The deformation can cause periodic patterns either (a) in the axial direction that maintains axisymmetry, or (b) in the circumferential direction that maintains the plane strain condition.

such as soft grippers [26]. Soft microfluidic channels made of elastomer through soft lithography or rapid prototyping have been shown to be advantageous as deformation of these channels are useful in actuating the valves between the pumps [27]. In addition, soft channels are encountered in polymeric hydrogels experiencing high strain and confined in granular medium for use as water reservoir in agriculture [28].

Bifurcation analysis of incompressible thick-walled tube under combined axial loading and external/internal pressure is discussed by Haughton and Ogden [29]. They studied the effect of wall-thickness which leads to non-homogeneous deformation. Sang et al. [30] performed the stability analysis of incompressible rubber tube under internal pressure using Gent's strain energy function. Recently, Liu [31] investigated the axial and circumferential modes of buckling in constrained incompressible cylindrical tube under compression and determine the critical thickness ratio for transition of mode types. Anani and Rahimi [32] discussed the stability analysis of functionally graded incompressible thick-walled cylindrical and spherical shells using extended version of Ogden's strain energy function. The wall-thickness has a significant influence on the stability of cylinder subjected to internal/external pressure. In particular, this motivates the investigation of the effect of displacement constraints along the outer surface, wall-thickness and material compressibility on critical pressure at which the instability occurs in the cylinder.

In the current work, we study large deformation of pressurised thick-walled hyperelastic compressible cylinder and investigate the onset of instability under internal pressure. By incorporating the compressible version of neo-Hookean constitutive model in the strain energy density function, the base state solutions are obtained for cylinders along azimuthal as well as axial direction. Both constrained and free boundary conditions are considered on the external surface of the cylinder. The bifurcation solutions are then obtained by perturbing the principal solutions with a small parameter (ϵ) using incremental deformation theory [33] along the circumferential and axial direction of the cylinder. The resulting incremental equations are solved numerically using the compound matrix method for computing critical value of inflating pressure. The buckling modes corresponding to the critical pressure along the axial and circumferential directions are investigated. Finally, the influence of stiffening the cylindrical tube along the axial direction with fibre reinforcement and its role on the elastic instabilities is studied.

1.1. Organisation of this manuscript

The remainder of this paper is organised as follows. In Section 2, we discuss the base state solution for the cylinder subjected to internal pressure under free as well as constrained boundary conditions on the outer surface. In Section 3, we derive the incremental differential equations by perturbation in the circumferential and axial direction. In Section 4, we derive the non-dimensional ordinary differential equations (ODEs) and evaluate the critical pressure that causes instability in circumferential as well as axial direction using compound matrix method and shooting method. Later in this section, we present a detailed discussion of numerical results also including the comparison of bifurcation solution in axial and circumferential direction. Finally, we conclude the work in Section 5 with the scope for potential future extensions. Supplementary mathematical derivations are given in the Appendix.

1.2. Notation used in this manuscript

Brackets: Two types of brackets are used. Round brackets () are used to define the functions applied on parameters or variables. Square brackets [ ] are used to clarify the order of operations in an algebraic expression.

Symbols: A variable typeset in a normal weight font represents a scalar. A lower-case bold weight font denotes a vector and bold weight upper-case font denotes a tensor. Matrix of a tensor is depicted by enclosing the tensor in square brackets. Tensor product of two second order tensors $\mathbf{A}$ and $\mathbf{B}$ is defined as either $[\mathbf{A} \otimes \mathbf{B}]_{ijkl} = [\mathbf{A}]_{ij}[\mathbf{B}]_{kl}$ or $[\mathbf{A} \boxtimes \mathbf{B}]_{ijkl} = [\mathbf{A}]_{ik}[\mathbf{B}]_{jl}$. Higher order tensors are written in bold calligraphic font with a superscript as $\mathcal{A}^{(i)}$, where superscript 'i' indicates that the function is differentiated $i + 1$ times. For example, $\mathcal{A}^{(1)} = \dfrac{\partial^2 \Omega}{\partial \mathbf{F} \partial \mathbf{F}}$ is a fourth order tensor. Operation of a fourth order tensor on a second order tensor is denoted as $[\mathcal{A}^{(1)} : \mathbf{A}]_{ij} = [\mathcal{A}^{(1)}]_{ijkl}[\mathbf{A}]_{kl}$. Inner product is defined as $\mathbf{A} \cdot \mathbf{B} = [\mathbf{A}]_{ij}[\mathbf{B}]_{ij}$. We use the word 'Div' to denote divergence in three dimensions. The term $\delta \mathbf{F}$ is used to represent the increment in $\mathbf{F}$.

Functions: $\det(\mathbf{F})$ denote the determinant of a tensor $\mathbf{F}$. $\mathrm{tr}(\mathbf{F})$ denote the trace of a tensor $\mathbf{F}$.
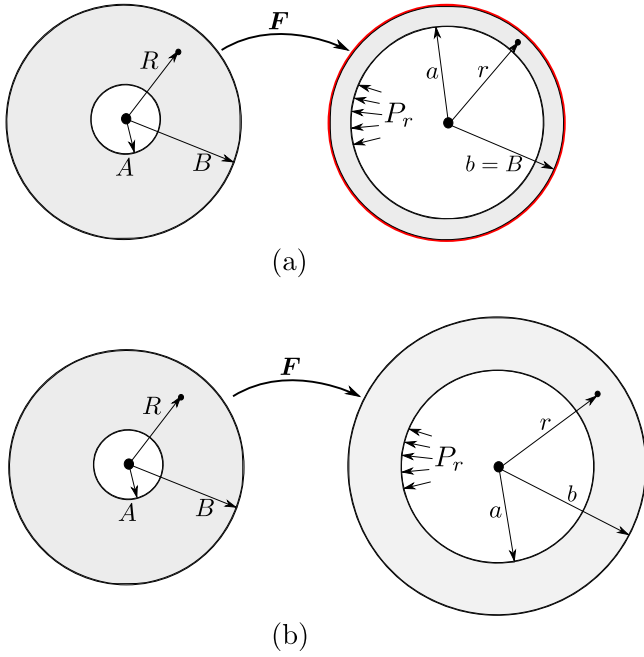
Fig. 2. Cross-section of the cylinder in the reference and deformed configurations corresponding to the two boundary conditions considered. The inner and outer radii are A and B that transform to a and b, respectively, due to an internal pressure P_r. (a) The outer surface is constrained forcing $b = B$. (b) The outer surface is free to expand.

2. Kinematics and principal solution

Consider an infinitely long thick cylinder with an internal radius A and external radius B in its stress-free reference configuration. The cylinder is deformed by an internal pressure P_r as shown in Fig. 2 under two types of boundary conditions (free and constrained) on the outer surface. Let the cylindrical coordinates in the reference configuration be denoted by (R, Θ, Z) and in the deformed configuration by (r, θ, z). In its deformed configuration, the internal radius of the cylinder is given by a and the external radius is b. For the constrained boundary condition on the outer surface, $b = B$. A plane strain problem is considered and therefore no dependence on the Z coordinate is considered. We also assume axisymmetry that removes any dependence on the Θ coordinate. We denote the deformation gradient by $\mathbf{F}$ and the right Cauchy–Green deformation tensor as $\mathbf{C} = \mathbf{F}^T \mathbf{F}$. For the current case of axisymmetric deformation, we can write the components of $\mathbf{F}$ in the cylindrical coordinate system as $[\mathbf{F}] = \text{diag}(\lambda_r, \lambda_\theta, \lambda_z)$ where the principal stretch ratios can be written as

$$\lambda_r = \frac{\partial r}{\partial R}, \qquad \lambda_\theta = \frac{r}{R}, \qquad \lambda_z = 1. \tag{2.1}$$

The deformation function in the radial direction $r(R)$ is an unknown.

2.1. Equilibrium and boundary conditions

The balance of linear momentum

$$\text{Div } \mathbf{P} = \mathbf{0}, \tag{2.2}$$

can be written in cylindrical coordinates for this axisymmetric case with no dependence of variables along the Z coordinate as

$$P'_{Rr} + \frac{1}{R} \left[P_{Rr} - P_{\Theta\theta} \right] = 0. \tag{2.3}$$

Here, $\mathbf{P}$ is the first Piola–Kirchhoff stress tensor with components $P_{ij} := [\mathbf{P}]_{ij}$ and a prime denotes derivatives with respect to R. There are no shear components of stress because of isotropy and $\mathbf{F}$ being diagonal

(axisymmetric deformation). For simplicity we use a compressible neo-Hookean energy density function for the hyperelastic material [34]

$$\Omega(I_1, I_3) = \frac{\mu}{2} \left[I_1 - 3 - \log I_3 \right] + \frac{\kappa}{4} \left[\log I_3 \right]^2, \tag{2.4}$$

where the scalar invariants are defined as $I_1 = \text{tr}(\mathbf{C}), I_3 = J^2 = [\det(\mathbf{F})]^2$, μ is the ground state shear modulus, and κ is a material parameter that relates to the ground state bulk modulus K as $\kappa = K/2 - \mu/3$. Using (2.4), the equilibrium Eq. (2.3) is rewritten as (with detailed derivations in Appendix A)

$$\frac{\partial}{\partial R} \left(\alpha \left[r' - \frac{1}{r'} \right] + \frac{2}{r'} \log \left(\frac{rr'}{R} \right) \right) = \frac{\alpha}{R} \left[\frac{r}{R} - r' \right]$$
$$+ \frac{1}{R} \left[\alpha - 2\log \left(\frac{rr'}{R} \right) \right] \left[\frac{1}{r'} - \frac{R}{r} \right]. \tag{2.5}$$

This is a second order ODE for the unknown $r(R)$ with $R \in [A, B]$. Note that here we have defined a dimensionless parameter $\alpha = \mu/\kappa$. In the linear elastic regime ($\mathbf{F} \approx \mathbf{I}$), the parameter α is written in terms of the Poisson's ratio ν as $\alpha = (1 - 2\nu)/\nu$ which implies that for $\alpha = 0$, the cylinder is incompressible. In order to assess the mechanical response for compressible cylinders, we perform computations for $\alpha > 0$.

2.1.1. Constrained boundary conditions

If the outer boundary of the cylinder is constrained as shown in Fig. 2a, then the displacement boundary condition over the external surface is

$$r = B, \qquad \text{at} \qquad R = B, \tag{2.6}$$

and the traction boundary condition over the inner surface is

$$-P_r = P_{Rr}, \qquad \text{at} \qquad R = A, \tag{2.7}$$

where P_r is internal pressure.

2.1.2. Free boundary conditions

If the outer boundary of the cylinder is free as shown in Fig. 2b, then the required traction boundary conditions are

$$-P_r = P_{Rr}, \quad \text{at} \quad R = A, \quad \text{and} \quad P_{Rr} = 0 \quad \text{at} \quad R = B. \tag{2.8}$$

2.2. Numerical pre-buckling solution

The second order ODE (2.5) can be rewritten as a system of two first order ODEs by defining $y_1 = r$ and $y_2 = r'$ as

$$\begin{bmatrix} 1 & 0 \\ 0 & \mathcal{W}_1 \end{bmatrix} \begin{bmatrix} y'_1 \\ y'_2 \end{bmatrix} = \begin{bmatrix} y_2 \\ \mathcal{W}_2 \end{bmatrix}, \tag{2.9}$$

where the coefficients $\mathcal{W}_1$ and $\mathcal{W}_2$ in (2.9) are

$$\mathcal{W}_1 = \alpha \left[1 + \frac{1}{y_2^2} \right] + \frac{2}{y_2^2} \left[1 - \log \left(\frac{y_1 y_2}{R} \right) \right],$$
$$\mathcal{W}_2 = \frac{\alpha}{R} \left[\frac{y_1}{R} - y_2 \right] + \frac{1}{R} \left[\alpha - 2\log \left(\frac{y_1 y_2}{R} \right) \right] \left[\frac{1}{y_2} - \frac{R}{y_1} \right] + 2 \left[\frac{1}{R y_2} - \frac{1}{y_1} \right]. \tag{2.10}$$

The corresponding boundary conditions transform to

$$\alpha \left[y_2 - \frac{1}{y_2} \right] + \frac{2}{y_2} \log \left(\frac{y_1 y_2}{R} \right) + \widetilde{P} = 0, \qquad \text{at} \quad R = A, \tag{2.11}$$

$$y_1 = B, \qquad \text{at} \quad R = B, \tag{2.12}$$

for the constrained outer surface and

$$\alpha \left[y_2 - \frac{1}{y_2} \right] + \frac{2}{y_2} \log \left(\frac{y_1 y_2}{R} \right) + \widetilde{P} = 0, \qquad \text{at} \quad R = A, \tag{2.13}$$

$$\alpha \left[y_2 - \frac{1}{y_2} \right] + \frac{2}{y_2} \log \left(\frac{y_1 y_2}{R} \right) = 0, \qquad \text{at} \quad R = B, \tag{2.14}$$
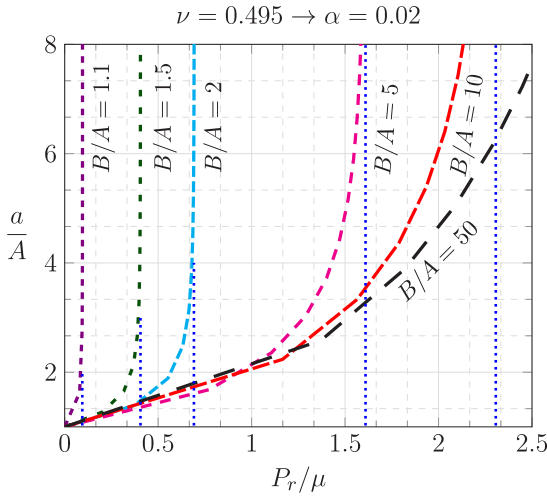
Fig. 3. The deformed dimensionless internal radius a/A (dilation) as a function of the dimensionless applied internal pressure P_r/μ for a range of cylinder thickness (B/A) for a nearly incompressible cylinder ($\alpha = 0.02 \rightarrow \nu = 0.495$). The plots are very close to those presented by Cheewaruangroj et al. [16] (Figure 2) for incompressible cylinders.

for the free outer surface of the cylinder. Here $\widetilde{P} = P_r/\kappa$ is the dimensionless internal pressure.

In order to validate our current model, we compare the predictions with existing results for inflation of an incompressible cylinder with free boundary. Eqs. (2.9)–(2.14) are solved using the bvp4c solver based on residual control in Matlab R2018a for $\alpha = 0.02$ (or $\nu = 0.495$), and for various cylinder thickness values, $B/A = 1.1, 1.5, \ldots, 50$. These results are presented in Fig. 3 and are in good agreement with the results reported by Cheewaruangroj et al. [16] for incompressible cylinders ($\nu = 0.5$). The plots show the variation of the deformed inner radius a/A (dilation) with respect to the normalised internal pressure. The contribution of κ term in (2.4) is very small as $J \rightarrow 1$ or $\log(J) \rightarrow 0$ for the parameter, $\alpha = 0.02$. We note the existence of a critical limiting pressure, $P_r = \mu \log(B/A)$ at which the divergence happens leading to massive changes in the radius for a minor change in the pressure (blue dotted line in Fig. 3). The critical limit of pressure is not observed as B/A tends to infinity.

Results for the deformation of compressible cylinders with free and constrained external boundaries are shown in Figs. 4 and 5, respectively. The plots show the variation of the deformed inner radius a/A with the internal applied pressure $\widetilde{P}$ for different values of the material parameter α.

Results of constrained and unconstrained cases show that the maximum dilation for any value of B/A decreases with increasing value of α. In the constrained case, the inner radius deforms less for smaller value of radius ratio (B/A) and this is due to the fixed boundary which causes resistance to dilation. As the wall-thickness increases, the deformation of inner radius increases due to less dilation resistance from the boundary constraints. For the constrained case, the variation of a/A with respect to internal pressure is nonlinear for lower values of α and becomes linear for higher values of α. This trend is markedly opposite in the unconstrained case shown in Fig. 4 due to the stress free boundary and the variation of a/A is almost linear for all values of α. This behaviour is in contrast to the nonlinear variation observed for the nearly incompressible case results shown in Fig. 3. Here, the thick cylinder deforms less as compared to thin cylinder for same amount of pressure and material/geometrical parameters.

When the limit $B/A \rightarrow \infty$, it corresponds to a cylindrical channel in an infinite space for which the influence of boundary is negligible and the deformation in the cylinder is identical for both constrained and unconstrained cases. We demonstrate this by choosing $B/A = 50$ in the simulations and it is observed that these results corresponding to lower

bound for unconstrained cases and upper bound for constrained cases converge in Figs. 4 and 5.

3. Incremental equations

In this section, we derive the partial differential equations that govern the instability behaviour of cylindrical channels subjected to internal pressure based on incremental theory. We follow the general framework of Haughton and Ogden [35] restricting our discussion to the compressible neo-Hookean model of Eq. (2.4). Consider small perturbations to the primary deformation (r, θ, z) scaled by a parameter $0 < \epsilon \ll 1$ such that the total deformation is

$$\hat{r} = r + \epsilon u, \quad \hat{\theta} = \theta + \epsilon v, \quad \text{and} \quad \hat{z} = z + \epsilon w, \tag{3.1}$$

and the associated first Piola–Kirchhoff stress tensor [33] is

$$\delta \mathbf{P} = \mathcal{A}^{(1)} \delta \mathbf{F} + \frac{1}{2} \mathcal{A}^{(2)} [\delta \mathbf{F}, \delta \mathbf{F}] + \cdots, \tag{3.2}$$

where $\delta \mathbf{F}$, $\delta \mathbf{P}$, and $\mathcal{A}^{(i)} = \dfrac{\partial^{i+1} \Omega}{\partial \mathbf{F}^{i+1}}$ are the incremental deformation gradient tensor, incremental first Piola–Kirchhoff tensor, and elastic moduli of the material, respectively. Upon ignoring the higher order terms in (3.2), the incremental first Piola–Kirchhoff stress tensor is given as

$$\delta \mathbf{P} = \mu \left[\delta \mathbf{F} + [\mathbf{F}^{-1}[\delta \mathbf{F}] \ \mathbf{F}^{-1}]^T \right] + 2\kappa \left[\mathbf{F}^{-T} \ \text{tr}(\mathbf{F}^{-1}[\delta \mathbf{F}]) - \log J [\mathbf{F}^{-1}[\delta \mathbf{F}] \ \mathbf{F}^{-1}]^T \right]. \tag{3.3}$$

The incremental equilibrium equation and the associated incremental boundary conditions are

$$\text{Div}(\delta \mathbf{P}) = \mathbf{0}, \tag{3.4a}$$

$$[\delta \mathbf{P}]\mathbf{N} = J P_r \mathbf{F}^{-T} [\delta \mathbf{F}]^T \mathbf{F}^{-T} \mathbf{N} - J P_r \text{tr} \left(\mathbf{F}^{-1}[\delta \mathbf{F}] \right) \mathbf{F}^{-T} \mathbf{N}. \tag{3.4b}$$

The expression of $\delta \mathbf{F}$, $\mathcal{A}^{(i)}$, and detailed mathematical derivations associated with Eqs. (3.3)–(3.4) are presented in Appendix A. In this work, we seek two types of bifurcation from the primary solution. The first one is a solution that satisfies the plane strain condition ($w = 0$) and causes perturbations in the radial–circumferential direction (i.e., r, θ coordinates). The second bifurcation problem is the perturbation of the solution along the radial–axial direction (i.e., r, z coordinates) and no variation along the circumferential coordinate, that is, $v = 0$. The bifurcation along the axial direction is also possible by perturbing the primary solution only along radial component of the cylinder i.e., $v = w = 0$ in contrast to the latter case of bifurcation.

3.1. Perturbation along the circumferential direction

We first apply small perturbations to the principal solution by choosing $0 < \epsilon \ll 1$ which satisfy the plane strain condition by considering $w = 0$ in Eq. (3.1). The functions u and v depend only on the coordinates (R, Θ). The associated two-dimensional deformation gradient is given by $\mathbf{F} = \text{diag}(\lambda_r, \lambda_\Theta)$, where λ_r and λ_θ are the principal stretches of prescribed deformation. Consider a sinusoidal perturbation as an ansatz

$$u(R, \Theta) = \Delta f(R) \cos(n\Theta), \quad \text{and} \quad v(R, \Theta) = \Delta g(R) \sin(n\Theta), \tag{3.5}$$

where 'n' denotes the wave number in circumferential direction. On substituting (3.5) in the equilibrium Eq. (3.4a) and collecting only $O(\epsilon)$ terms, we obtain the incremental differential equations for the functions Δf and Δg as

$$\Delta f'' = -\frac{1}{\tilde{a}_1} \left[\tilde{a}_2 \Delta f' + \tilde{a}_3 \Delta f + \tilde{a}_4 \Delta g' + \tilde{a}_5 \Delta g \right], \tag{3.6a}$$

$$\Delta g'' = -\frac{1}{\tilde{b}_1} \left[\tilde{b}_2 \Delta g' + \tilde{b}_3 \Delta g + \tilde{b}_4 \Delta f' + \tilde{b}_5 \Delta f \right]. \tag{3.6b}$$
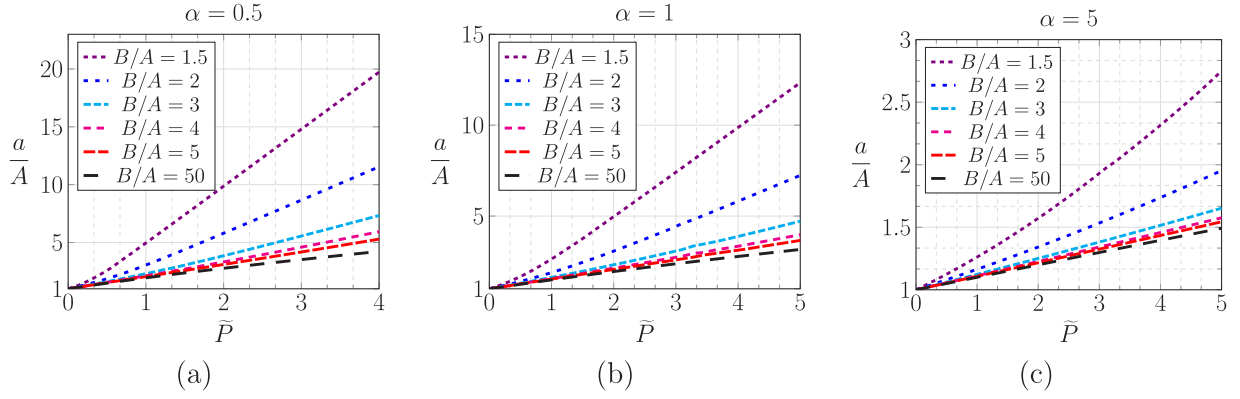
Fig. 4. Free inflation: Variation of the deformed internal radius a/A with the applied internal pressure $\widetilde{P}$ for different values of radius ratio (B/A) and material parameter (a) $\alpha = 0.5$ (b) $\alpha = 1$, (c) $\alpha = 5$.
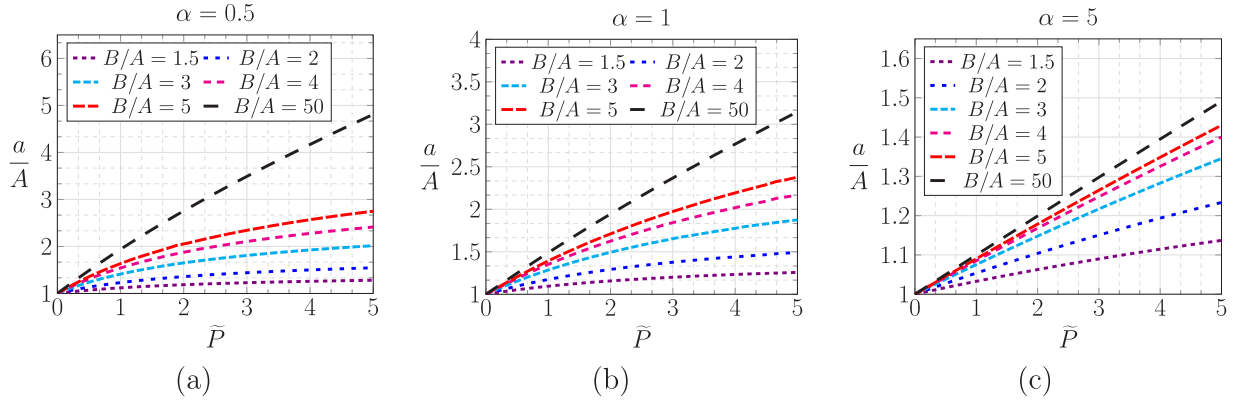

Fig. 5. Constrained inflation: Variation of the deformed internal radius a/A with the applied internal pressure $\widetilde{P}$ for different values of radius ratio (B/A) and material parameter (a) $\alpha = 0.5$ (b) $\alpha = 1$, (c) $\alpha = 5$.

The inner and outer boundary conditions for constrained cylinder are derived by making use of (3.4b), and collecting the linear order terms in ϵ

$$\left. \begin{array}{l} \tilde{a}_{11}\Delta f + \tilde{a}_{22}\Delta f' + \tilde{a}_{33}\Delta g = 0, \\ \tilde{b}_{11}\Delta f + \tilde{b}_{22}\Delta g' = 0, \end{array} \right\} \quad \text{at } R = A, \tag{3.7a}$$

$$\Delta f = \Delta g = 0, \qquad \text{at } R = B. \tag{3.7b}$$

The coefficients $\tilde{a}_1 - \tilde{a}_5$, $\tilde{b}_1 - \tilde{b}_5$ in (3.6) and $\tilde{a}_{11} - \tilde{a}_{33}$, $\tilde{b}_{11} - \tilde{b}_{22}$ in the boundary conditions (3.7) are given in Appendix B.

3.2. Perturbation along the axial direction

In this section, we apply small increments $(0 < \epsilon \ll 1)$ to the principal solution with perturbations along the axial direction satisfying axisymmetry by considering $v = 0$ in Eq. (3.1). The functions u and w depend only on the coordinates (R, Z). The associated deformation gradient in terms of principal stretches is given as $\mathbf{F} = \mathrm{diag}(\lambda_r, \lambda_\theta, 1)$. We consider the following ansatz

$$u(R, Z) = \Delta \bar{f}(R) \cos\left(2\pi m \frac{Z}{L}\right), \quad \text{and} \quad w(R, Z) = \Delta \bar{h}(R) \sin\left(2\pi m \frac{Z}{L}\right). \tag{3.8}$$

Here, 'm' represents the wavenumber along the axial direction. We take the analysis domain in Z direction as $0 \le Z \le L$, where L is the length of the cylinder. Upon substituting (3.8) in the equilibrium Eq. (3.4a) and collecting $O(\epsilon)$ terms, we obtain the incremental ODEs for $\Delta \bar{f}$ and

$\Delta \bar{h}$ as

$$\begin{aligned} \Delta \bar{f}'' &= -\frac{1}{c_1}\left[c_2\Delta \bar{f}' + c_3\Delta \bar{f} + c_4\Delta \bar{h}' + c_5\Delta \bar{h}\right], \\ \Delta \bar{h}'' &= -\frac{1}{d_1}\left[d_2\Delta \bar{h}' + d_3\Delta \bar{h} + d_4\Delta \bar{f}' + d_5\Delta \bar{f}\right]. \end{aligned} \tag{3.9}$$

The boundary condition (3.4b) for constrained cylinder is given by

$$\left. \begin{array}{l} c_{11}\Delta \bar{f} + c_{22}\Delta \bar{f}' + c_{33}\Delta \bar{h} = 0, \\ d_{11}\Delta \bar{f} + d_{44}\Delta \bar{h}' = 0, \end{array} \right\} \quad \text{at} \quad R = A, \tag{3.10a}$$

$$\Delta \bar{f} = \Delta \bar{h} = 0, \qquad \text{at} \qquad R = B, \tag{3.10b}$$

where the coefficients $c_1 - c_5$, $d_1 - d_5$ associated with (3.9) and $c_{11} - c_{33}$, $d_{11} - d_{44}$ associated with (3.10) are given in Appendix B.

As a special case, we perform the bifurcation analysis in the axial direction of cylinder by perturbing only radial component. For this, we consider $v = w = 0$ in Eq. (3.1) and consider the perturbation $\widetilde{r}(R, Z) = r(R) + \epsilon \Delta \widetilde{f}(R) \cos\left(\widetilde{m} 2\pi Z/L\right)$. This is attributed to the presence of only radial strain that resists the applied pressure. The radial perturbation alone results in second order incremental ODE i.e., function of $\Delta \widetilde{f}$ which is obtained by substituting $\tilde{a}_4 = \tilde{a}_5 = 0$ in (3.6a). The inner and outer boundary condition associated with this case is obtained by substituting $\Delta \bar{h} = \Delta \bar{h}' = 0$ in (3.10). The mathematical equations are provided in Appendix B.5

4. Numerical solution and discussion

The ODEs derived in Sections 3.1–3.2 are reformulated in Appendix B for ease of numerical solution. We compute the numerical solution using the classical shooting method (or determinantal method) [29,36] as well as the compound matrix method [37–39].
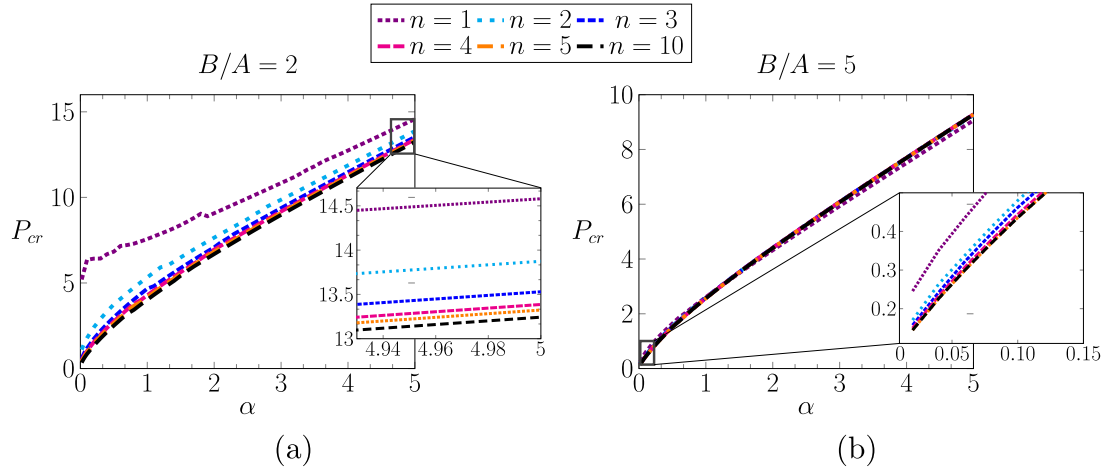
Fig. 6. Dependence of the critical dimensionless pressure on the compressibility factor α for bifurcation in the circumferential direction with mode number n of a constrained cylinder at (a) $B/A = 2$, and (b) $B/A = 5$.

4.1. Comparison of the numerical schemes

Shooting method and the compound matrix method are implemented in the Matlab 2018a programming environment. The `ode45` ODE solver that implements an explicit Runge–Kutta method and `fminsearchbnd` optimisation subroutine [40] based on Nelder–Mead simplex algorithm is used. A tolerance value of 10^{-8} is chosen to compute the bifurcation solution. Both the methods compute the same results, but the compound matrix method is approximately four times faster than the shooting method. As an example, on a computer with an 8 core, 2.10 GHz processor and 48 GB of RAM, computation of the curve corresponding to $B/A = 2$, $n = 1$ in Fig. 6a takes 142 seconds using the compound matrix method and 666 seconds using the standard shooting method.

4.2. Bifurcation of solution for a constrained cylinder

The dimensionless critical pressure (defined as P_{cr}) to induce bifurcation in the circumferential direction is computed numerically by solving the Eqs. (B.2) and (B.3) subjected to the boundary conditions (B.4) and (B.5). Variation of the critical pressure with respect to material parameter α for fixed radius ratio is shown in Fig. 6. The P_{cr} monotonically increases with α and its magnitude decreases with the increase in wall-thickness. The imposed boundary conditions cause thicker channel to experience instability at a lower critical pressure than the thin cylindrical channel. For thin cylinder case ($B/A = 2$), the bifurcation solution of $n = 1$ requires higher pressure than the other modes suggesting that a bifurcation with higher mode number is energetically preferred to induce the instability. For thick cylinder case ($B/A = 5$), all the modes are close to each other. The higher modes are preferred for low values of α and the first mode is preferred for higher values of α as shown in Fig. 6b. We are able to compute the solutions for value of α as low as 0.02 which correspond to a ground state Poisson's ratio of 0.495 and is comparable to an incompressible material. The stable region for all the modes with $B/A = 2$, and $\alpha = 1$ is shown in Fig. 7 which indicates the absence of bifurcation below the critical pressure, $P_{cr} \approx 4$.

The critical pressure to induce bifurcation in the axial direction is computed by the numerical solution of Eqs. (B.9) subjected to the boundary conditions (B.10). Here, $k = 2\pi m(B/L)$ is a dimensionless wavenumber (see Appendix B) and can take any positive real value as opposed to n that needs to be an integer. Fig. 8 shows the variation of the critical pressure against the material parameter α. Again, the higher modes are energetically preferred over lower modes and the bifurcation solution is shown up to $k = 10$ beyond which there is not much

difference in the higher mode solutions. The red solid pressure curve corresponds to the critical pressure obtained by numerical solution of (B.12) subjected to the boundary conditions (B.13) and (B.14). This bifurcation is obtained for the mode $\widetilde{k} = 10$ for $B/A = 2, 5$. The non-dimensional number $\widetilde{k}$ is a rescaled parameter defined as $\widetilde{k} = 2\pi\widetilde{m}(B/L)$ corresponding to the special case described in Section 3.2. In this case, only an incremental radial strain is induced by the critical pressure which results in the bifurcation solution that corresponds to $\widetilde{k} = 10$. The critical pressure evaluated in the radial perturbation case is higher than the value obtained for the radial and axial perturbation. Thus, the bifurcation solution that corresponds to $k = 10$ is energetically preferred over the bifurcation solution of $\widetilde{k} = 10$ to induce the instability along the axial direction.

The variation of critical pressure with α, B/A and k is similar to that seen for the circumferential bifurcation case. However, the magnitude of the critical pressure obtained is smaller for all the values of the parameters chosen. For the same parameters of $B/A = 2$ and $\alpha = 1$ with constrained boundary condition (B.10), the pressure curve converge to limiting value of $P_{cr} \approx 3.3$ when plotted against k. Thus, a cylinder with constrained boundary subjected to an internal pressure is likely to develop instabilities along the axial direction.

4.3. Bifurcation of solution for cylinder with a free external boundary

The critical pressure to induce bifurcation in the circumferential direction is computed numerically by solving Eqs. (B.2) and (B.3) subjected to stress free boundary conditions (B.6) and (B.7). Variation of P_{cr} with respect to the material parameter α for different modes is shown in Fig. 9. The critical pressure rises with the increase in compressibility factor α and tend to converge when $\alpha(= 0.02)$ become too small. The behaviour of bifurcation curves in this case is different from constrained case when compared in terms of mode numbers. For the thin cylinders $B/A = 2$, no solution is obtained for $n = 1$ and, the mode $n = 2$ requires less energy in inducing instability when compared to higher modes as evident from Fig. 9a. For the thick cylinders, instability appears only for $n \geq 3$ as no solution is obtained for $n = 1, 2$. The value of critical pressure for all the modes converges for higher value of B/A and there is not much difference in the bifurcation solution.

The critical pressure to induce bifurcation in the axial direction is computed by the numerical solution of Eqs. (B.9) along with the boundary conditions (B.10a) and (B.11). Variation of P_{cr} versus material parameter α is shown in Fig. 10. Similar to the constrained cylinder case, increasing the value of α leads to rise in the value of the critical pressure. The dependence of critical pressure on radius
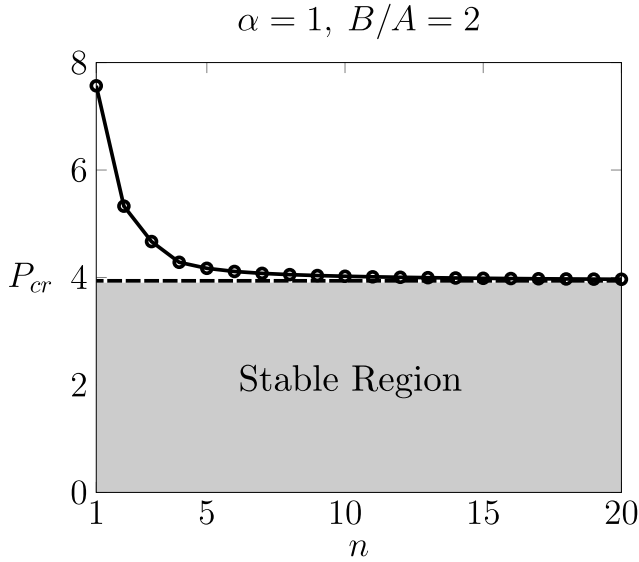
$$\alpha = 1, \ B/A = 2$$

Fig. 7. Variation of the critical dimensionless pressure for circumferential bifurcation of a constrained cylinder with respect to mode number n. It is seen that the curve asymptotically converges to a certain critical pressure value for all higher modes.

ratio B/A is opposite to that observed in the case of constrained axial cylinder. The magnitude of P_{cr} increases with the value of B/A as shown in Fig. 10b. This shows that thick cylinders have more stable behaviour at high inflation pressure and attain wrinkled configuration at a higher value of critical pressure due to large material resistance as compared to thin cylinders. Again, we have shown the onset of axial instability by perturbing only the radial component in (3.8) as discussed in Section 4.2. The red solid pressure curve shown in Fig. 10 is the lowest critical pressure curve obtained by the numerical solution of (B.12) subjected to unconstrained boundary condition (B.13) and (B.15) and corresponds to the mode number $\tilde{k} = 0.1$. This pressure is much higher due to resistance only from the radial strain as compared to the bifurcation solution of $k = 0.1$ for $B/A = 2, 5$. Here, the lowest wavenumber corresponds to $k = 0.1$ is energetically preferred over the other modes for inducing instability along the axial direction of the cylinder. Note that bifurcation solution exist for $k < 0.1$, however the bifurcation curves are very close to each other for lower values of k. Furthermore, bifurcation for lower modes along axial direction requires less critical pressure than that for circumferential direction suggesting that buckling in axial direction is energetically preferred. Similar trends for threshold pressure with wave length and material stiffness (μ) for incompressible cylinder with unconstrained boundary are reported by Cheewaruangroj et al. [16]. They estimated numerically and experimentally the critical pressure for incompressible thick cylinders ($B/A = 1000$) to be $(P/\mu)_{cr} = 2.05$. Using the same geometric parameters, we have calculated the critical value of pressure for axial cylinder made up of neo-Hookean compressible material subjected to unconstrained boundary conditions. The critical pressure for thick cylinders $B/A = 1000$ at lowest mode $k = 0.1$ with lowest material parameter value $\alpha = 0.02$ (slightly incompressible) is calculated as $(P/\kappa)_{cr}$ or $P_{cr} = 0.057$ which is equivalent to $(P/\mu)_{cr} = 2.53$.

4.4. Comparison of the bifurcation in the axial and circumferential directions

For both the constrained and free cylinders, it is observed that the critical bifurcation pressure in the axial direction is lower than the circumferential direction (see Figs. 6–10). In order to design cylindrical systems that can lead to pattern formation (bifurcation) upon inflation in the circumferential direction, one needs to increase the stiffness in the axial direction.

4.4.1. Stiffening of the axial direction

Consider the cylinder to be made of an anisotropic (transversely isotropic) material with an additional stiffness along a vector **a** in the reference configuration (for example, by introduction of continuously distributed fibres orientated along the vector **a**). For this case, we use the elastic strain energy density function [41]

$$\Omega^*(I_1, I_3, I_4) = \frac{\mu}{2}\left[I_1 - 3 - \log I_3\right] + \frac{\kappa}{4}\left[\log I_3\right]^2 + \Omega_f(I_4), \quad (4.1)$$

where $\Omega_f(I_4) = \frac{k_1}{2k_2}\left[\exp[k_2[I_4 - 1]^2] - 1\right]$ is the energy due to fibre reinforcement, $k_1 > 0$ is a parameter with units of stress, and $k_2 > 0$ is dimensionless parameter. The invariant $I_4 = \mathbf{a} \cdot \mathbf{Ca}$ represents the square of stretch in direction of anisotropy. In this case, the incremental dimensionless first Piola–Kirchhoff stress tensor is obtained as

$$\begin{aligned}\frac{\delta \mathbf{P}}{\kappa} =& \alpha\left[\delta\mathbf{F} + [\mathbf{F}^{-1}[\delta\mathbf{F}]\mathbf{F}^{-1}]^T\right] + 2\left[\mathbf{F}^{-T}\mathrm{tr}(\mathbf{F}^{-1}[\delta\mathbf{F}]) - \log J[\mathbf{F}^{-1}[\delta\mathbf{F}]\mathbf{F}^{-1}]^T\right] \\ & + 2\bar{k}_1 \exp\left[k_2[I_4 - 1]^2\right]\left[1 + 2k_2[I_4 - 1]\right]\left[\mathbf{a}\otimes\mathbf{Fa}\right]\left[\mathrm{tr}\left(\delta\mathbf{F}^T[\mathbf{a}\otimes\mathbf{Fa}]\right)\right] \\ & + 2\bar{k}_1[I_4 - 1]\exp\left[k_2[I_4 - 1]^2\right][\mathbf{a}\otimes\mathbf{a}]\,\mathrm{tr}(\delta\mathbf{F}^T), \quad (4.2)\end{aligned}$$

where $\bar{k}_1 = k_1/\kappa$ is a dimensionless parameter. In our problem, we assume plane strain and that the anisotropy is orientated along the axis of the cylinder that results in $I_4 = \lambda_Z^2 = 1$ and we obtain

$$\begin{aligned}\frac{\delta\mathbf{P}}{\kappa} =& \alpha\left[\delta\mathbf{F} + [\mathbf{F}^{-1}[\delta\mathbf{F}]\ \mathbf{F}^{-1}]^T\right] \\ & + 2\left[\mathbf{F}^{-T}\ \mathrm{tr}(\mathbf{F}^{-1}[\delta\mathbf{F}]) - \log J[\mathbf{F}^{-1}[\delta\mathbf{F}]\ \mathbf{F}^{-1}]^T\right] \\ & + 2\bar{k}_1\left[\mathbf{a}\otimes\mathbf{Fa}\right]\left[\mathrm{tr}\left(\delta\mathbf{F}^T[\mathbf{a}\otimes\mathbf{Fa}]\right)\right]. \quad (4.3)\end{aligned}$$

Auxiliary calculations to arrive at the above equations are provided in Appendix C.

The stress at a material point not only depends on the deformation gradient **F** but also the fibre direction **a**. For the cylinder with unit axial stretch ($\lambda_Z = 1$), the incremental stress corresponding to fibre term is independent of the dimensionless parameter k_2. The influence of stiffening along the axial coordinate on the critical pressure is studied for constrained and unconstrained boundary conditions. Table 1 shows the critical pressure results of constrained case of axially stiffened cylinder for different values of α and cylinder radius ratio. We note that the lowest mode is sensitive to geometry of the cylinder and changes with B/A. Table 1 also compares the P_{cr} values of axial stiffened cylinder with the regular cylinder results. The stiffening in axial direction has no effect on the critical pressure P_{cr} (hoop) which is responsible for circumferential bifurcation. For the constrained cylinder case, the fibre reinforcement in axial direction results in the increase of P_{cr} (fibre axial) which is higher than the P_{cr} (hoop). The stiffening of axial direction leads to the bifurcation along the circumferential direction and provides an approach for tailoring the bifurcation characteristics of such systems. Results also show that as α increases, we need higher stiffening (a higher $\bar{k}_1$ value) to enhance the critical pressure. However, in unconstrained cylinder, the stiffening along axial coordinate has no significant effect on critical pressure even for very high stiffening value ($\bar{k}_1 = 100$) as shown in Table 2. We present representative results for $\alpha = 1$ but similar results are obtained for other α values. The bifurcation always occurs at lower value of critical pressure in axial direction when compared to circumferential direction for unconstrained cylinder as discussed in the previous Section 4.4.

5. Conclusion

In summary, we have studied large deformation in internally pressurised thick-walled compressible cylinders made up of soft material due to their widespread applications in biomedical implants, additively manufactured metamaterials, highly flexible/stretchable electronics, soft microfluidic channels and soft robotics.
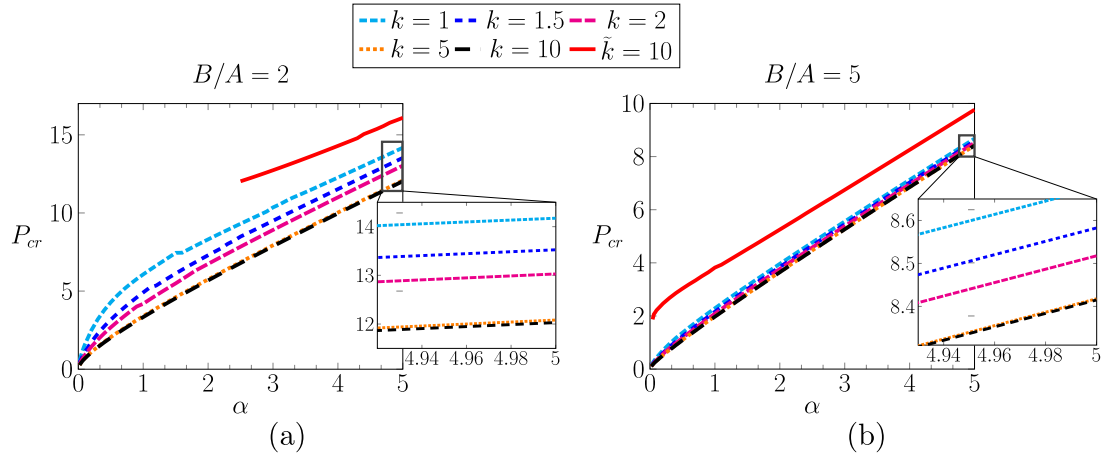
Fig. 8. Dependence of the critical dimensionless pressure on the compressibility factor α for bifurcation in the axial direction of a constrained cylinder at (a) $B/A = 2$, and (b) $B/A = 5$. The pressure curve associated with higher modes are energetically preferred.
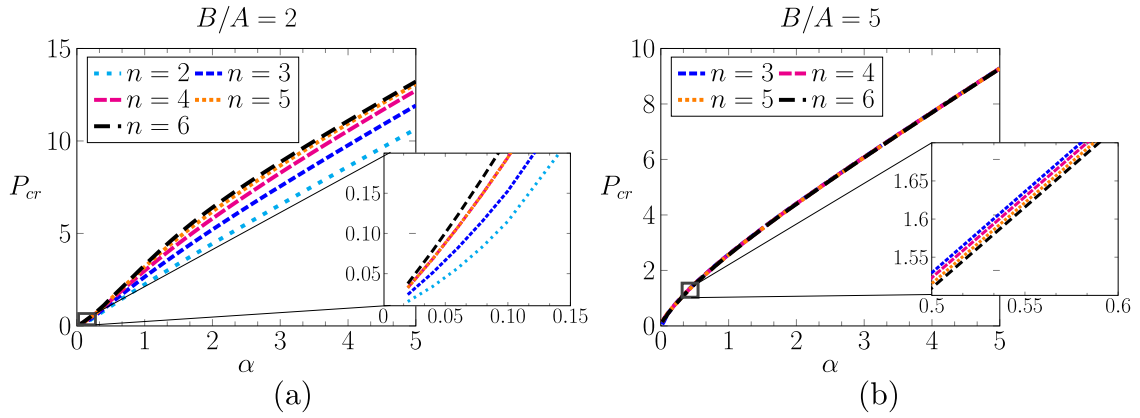

Fig. 9. Critical dimensionless pressure variation against compressibility factor for unconstrained cylinder perturbed along circumferential direction at (a) $B/A = 2$, and (b) $B/A = 5$.
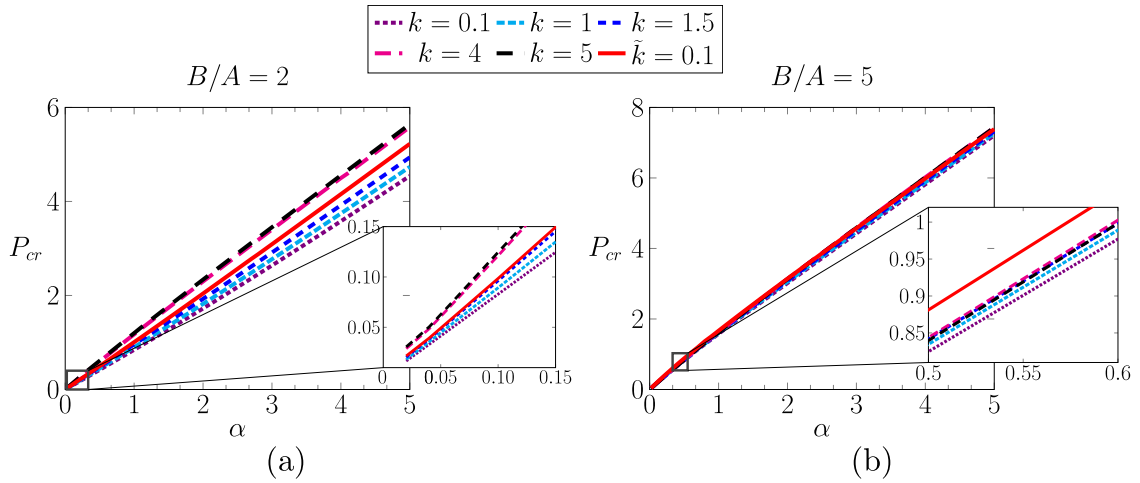

Fig. 10. Critical dimensionless pressure variation against compressibility factor for axially perturbed unconstrained cylinder at (a) $B/A = 2$, and (b) $B/A = 5$. The pressure curve associated with $k = 0.1$ is energetically preferred.

The internal pressure leads to elastic instability in thick-walled compressible cylindrical channels along the circumferential or axial direction. Incremental deformation theory is applied to derive the governing PDEs for the cylindrical channel. Two types of boundary conditions for the external surface of the cylinder are studied, namely, constrained and unconstrained to comprehend the bifurcation phenomena in the

circumferential and axial direction. The resulting incremental differential equations are obtained by perturbing the primary solution along the radial–circumferential as well as radial–axial direction. These equations are numerically solved for both the boundary conditions using compound matrix method and shooting method (or determinant method) to obtain the critical internal pressure which induces instability. We have also investigated the elastic instability in axial direction by perturbing

Table 1

Comparison of critical dimensionless bifurcation pressure values for isotropic and anisotropic constrained cylinders. P_{cr} for circumferential bifurcation remains unchanged but P_{cr} for axial bifurcation changes on the introduction of anisotropy.

B/A	$\alpha = 1$			$\alpha = 5$		
	P_{cr} (hoop)	P_{cr} (axial) isotropic	P_{cr} (axial) fibres	P_{cr} (hoop)	P_{cr} (axial) isotropic	P_{cr} (axial) fibres
1.5	5.81	4.90	6.70 ($\bar{k}_1 = 2$)	18.20	16.87	20.30 ($\bar{k}_1 = 15$)
	($n = 25$)	($k = 25$)	($k = 25$)	($n = 25$)	($k = 20$)	($k = 20$)
2	3.97	3.34	4.17 ($\bar{k}_1 = 2$)	13.22	12.03	13.94 ($\bar{k}_1 = 25$)
	($n = 20$)	($k = 10$)	($k = 10$)	($n = 15$)	($k = 10$)	($k = 10$)
5	2.56	1.98	2.61 ($\bar{k}_1 = 15$)	9.28	8.41	9.02 ($\bar{k}_1 = 50$)
	($n = 5$)	($k = 5$)	($k = 5$)	($n = 5$)	($k = 5$)	($k = 5$)

Table 2

Comparison of critical dimensionless bifurcation pressure values for isotropic and anisotropic unconstrained cylinders. P_{cr} for circumferential bifurcation remains unchanged but P_{cr} for axial bifurcation changes on the introduction of anisotropy. The compressibility factor is chosen to be $\alpha = 1$.

B/A	P_{cr} (hoop)	P_{cr} (isotropic, axial)	P_{cr} ($\bar{k}_1 = 100$) (fibres, axial)
1.5	1.17	0.51	0.64
	($n = 2$)	($k = 0.1$)	($k = 0.1$)
2	2.04	0.84	1.002
	($n = 1$)	($k = 0.1$)	($k = 0.1$)
5	2.22	1.58	1.67
	($n = 1$)	($k = 0.1$)	($k = 0.1$)

the primary solution only along the radial component of the cylinder. This results in higher critical pressure as compared to the critical pressure obtained through generalised radial–axial perturbation for both the boundaries considered. The effect of radius ratio (wall-thickness), compressibility factor and boundary conditions on the critical inflating pressure are systematically studied.

We also demonstrate that the numerical solutions of the resulting ODEs can be computed almost four times faster using the compound matrix method as compared to the standard shooting method. We observe that the pressure curves associated with constrained external surface have shown opposite behaviour than stress free external surface. The magnitude of critical pressure decreases with the increase of radius ratio due to the fixed boundary conditions in the constrained cylinder which causes thicker channels to experience instability at lower critical pressure than thin cylinders. Whereas, the critical pressure increases with the radius ratio in the unconstrained boundary condition case. The pressure curves monotonically increase with the increase in the value of material parameter α for all considered cases. For constrained cylinder, the pressure curves corresponds to higher wavenumber are energetically preferred. The explicit value of critical pressure is difficult to be obtained as the pressure curves associated with higher wavenumber are very close to each other, thus the stable region for the optimised working pressure is provided in which bifurcation is absent. The opposite behaviour is shown by unconstrained cylinder case where the lower modes are energetically preferred. Our computations reveal that for the lowest stable mode, the critical pressure that causes bifurcation in the axial direction is always lower than the critical pressure that causes bifurcation in the circumferential direction. However, this observation does not hold when the axial direction is stiffened with the fibres. The reinforcement of fibres in axial direction causes the bifurcation along the circumferential direction is more preferable in constrained cylinders whereas reinforcement have very less effect on bifurcation solution for unconstrained cylinders. We have restricted ourselves to determine the threshold pressure, but a post-bifurcation analysis may provide insights on the amplitude of wrinkles and stability of wrinkled solution. These avenues are currently under investigation.

Appendix A. Incremental stress and traction condition

The incremental stress (3.2) is rewritten in index notation as

$$[\delta \mathbf{P}]_{ij} = \mathcal{A}^{(1)}_{ijkl} \, [\delta \mathbf{F}]_{kl}, \tag{A.1}$$

where $\mathcal{A}^{(1)}_{ijkl}$ is the first order elastic moduli given by

$$
\begin{aligned}
\mathcal{A}^{(1)}_{ijkl} &= \mu \left[\delta_{ik}\delta_{jl} - \left[\mathbb{T}[-\mathbf{F}^{-1} \boxtimes \mathbf{F}^{-T}] \right]_{ijkl} \right] + 2\kappa \left[[\mathbf{F}^{-T}]_{ij} [\mathbf{F}^{-T}]_{kl} \right. \\
&\quad \left. + \log J \; \left[\mathbb{T}[-\mathbf{F}^{-1} \boxtimes \mathbf{F}^{-T}] \right]_{ijkl} \right], \\
&= \mu \left[\delta_{ik}\delta_{jl} + F^{-1}_{jk} F^{-T}_{il} \right] + 2\kappa \left[F^{-T}_{ij} F^{-T}_{kl} - \log J [F^{-1}_{jk} F^{-T}_{il}] \right],
\end{aligned}
\tag{A.2}
$$

and the associated deformation gradient is defined by using (3.1) as

$$
\mathbf{F} + \delta \mathbf{F} =
\begin{bmatrix}
\dfrac{\partial \hat{r}}{\partial R} & \dfrac{1}{R}\dfrac{\partial \hat{r}}{\partial \Theta} & \dfrac{\partial \hat{r}}{\partial Z} \\[8pt]
\hat{r}\dfrac{\partial \hat{\theta}}{\partial R} & \dfrac{\hat{r}}{R}\dfrac{\partial \hat{\theta}}{\partial \Theta} & \hat{r}\dfrac{\partial \hat{\theta}}{\partial Z} \\[8pt]
\dfrac{\partial \hat{z}}{\partial R} & \dfrac{1}{R}\dfrac{\partial \hat{z}}{\partial \Theta} & \dfrac{\partial \hat{z}}{\partial Z}
\end{bmatrix}.
\tag{A.3}
$$

Using (A.1), the Piola Kirchhoff stress is obtain as

$$
\begin{aligned}
[\delta \mathbf{P}]_{ij} &= \left[\mu \left[\delta_{ik}\delta_{jl} + F^{-1}_{jk} F^{-T}_{il} \right] + 2\kappa \left[F^{-T}_{ij} F^{-T}_{kl} - \log J [F^{-1}_{jk} F^{-T}_{il}] \right] \right] [\delta \mathbf{F}]_{kl}, \\
&= \mu \left[[\delta \mathbf{F}]_{ij} + [\mathbf{F}^{-1}[\delta \mathbf{F}]\mathbf{F}^{-1}]_{ji} \right] + 2\kappa \left[F^{-T}_{ij} \; [F^{-T}_{kl}[\delta \mathbf{F}]_{kl} \right. \\
&\quad \left. - \log J [\mathbf{F}^{-1}[\delta \mathbf{F}]\mathbf{F}^{-1}]_{ji} \right], \\
&= \mu \left[[\delta \mathbf{F}]_{ij} + [\mathbf{F}^{-1}[\delta \mathbf{F}]\mathbf{F}^{-1}]^T_{ij} \right] \\
&\quad + 2\kappa \left[F^{-T}_{ij} \; [\mathbf{F}^{-1}[\delta \mathbf{F}]]_{kk} - \log J [\mathbf{F}^{-1}[\delta \mathbf{F}]\mathbf{F}^{-1}]^T_{ij} \right].
\end{aligned}
\tag{A.4}
$$

Using (A.4), the Piola stress in direct notation is

$$
\delta \mathbf{P} = \mu \left[\delta \mathbf{F} + [\mathbf{F}^{-1}[\delta \mathbf{F}] \; \mathbf{F}^{-1}]^T \right] + 2\kappa \left[\mathbf{F}^{-T} \, \mathrm{tr}\left(\mathbf{F}^{-1}[\delta \mathbf{F}] \right) - \log J [\mathbf{F}^{-1}[\delta \mathbf{F}] \; \mathbf{F}^{-1}]^T \right].
\tag{A.5}
$$

Balance of traction in the current configuration subjected to internal pressure is

$$\boldsymbol{\sigma} \mathbf{n} = -P_r \mathbf{n}, \tag{A.6}$$

where $\boldsymbol{\sigma}$ is the Cauchy stress tensor, P_r is the internal pressure and $\mathbf{n}$ is the unit outward normal in the current configuration. This can be rewritten in the reference configuration as

$$\mathbf{P} \mathbf{N} = -J P_r \mathbf{F}^{-T} \mathbf{N}, \tag{A.7}$$

where $\mathbf{N}$ is the unit outward normal in the reference configuration. Using transformation (A.7), the incremental traction condition for inflating cylinder is given as

$$[\mathbf{P} + \delta \mathbf{P}]\mathbf{N} = -\left[J + \frac{\partial J}{\partial \mathbf{F}} \cdot \delta \mathbf{F} \right] \left[P_r + d P_r \right] \left[\mathbf{F}^{-T} + \frac{\partial \mathbf{F}^{-T}}{\partial \mathbf{F}} \cdot \delta \mathbf{F} \right] \mathbf{N},$$

$$= -\left[JP_r + J\,dP_r + P_r\left[\frac{\partial J}{\partial \mathbf{F}}\cdot\delta\mathbf{F}\right]\right]\left[\mathbf{F}^{-T} + \frac{\partial \mathbf{F}^{-T}}{\partial \mathbf{F}}\cdot\delta\mathbf{F}\right]\mathbf{N},$$

$$= -\left[JP_r\mathbf{F}^{-T}\mathbf{N} + J\,dP_r\mathbf{F}^{-T}\mathbf{N} + JP_r\left[\frac{\partial \mathbf{F}^{-T}}{\partial \mathbf{F}}\cdot\delta\mathbf{F}\right]\mathbf{N}\right.$$
$$\left. + P_r\left[\frac{\partial J}{\partial \mathbf{F}}\cdot\delta\mathbf{F}\right]\mathbf{F}^{-T}\mathbf{N}\right], \qquad (A.8)$$

where $(\cdot)$ represent the inner product. Eq. (A.8) results in

$$[\delta\mathbf{P}]\mathbf{N} = -JP_r\left[-\mathbb{T}\left[\mathbf{F}^{-1}\boxtimes\mathbf{F}^{-T}\right]\cdot[\delta\mathbf{F}]\right]\mathbf{N} - J\,dP_r\mathbf{F}^{-T}\mathbf{N}$$
$$- P_r\left[\det(\mathbf{F})\mathbf{F}^{-T}\cdot[\delta\mathbf{F}]\right]\mathbf{F}^{-T}\mathbf{N},$$

$$= -JP_r\left[-\left[F_{jk}^{-1}F_{il}^{-T}\right][\delta\mathbf{F}]_{kl}\right]N_j - J\,dP_rF_{ij}^{-T}N_j$$
$$- JP_r\,\mathrm{tr}(\mathbf{F}^{-1}[\delta\mathbf{F}])F_{ij}^{-T}N_j,$$

$$= JP_r\left[F_{il}^{-T}\,[\delta\mathbf{F}]_{lk}^T\,F_{kj}^{-T}\right]N_j - J\,dP_rF_{ij}^{-T}N_j$$
$$- JP_r\,\mathrm{tr}(\mathbf{F}^{-1}[\delta\mathbf{F}])F_{ij}^{-T}N_j. \qquad (A.9)$$

Eq. (A.9) can be written in direct notation as

$$[\delta\mathbf{P}]\mathbf{N} = JP_r\mathbf{F}^{-T}\,[\delta\mathbf{F}]^T\,\mathbf{F}^{-T}\mathbf{N} - J\,dP_r\mathbf{F}^{-T}\mathbf{N} - JP_r\,\mathrm{tr}(\mathbf{F}^{-1}[\delta\mathbf{F}])\mathbf{FN}. \quad (A.10)$$

Appendix B. Reformulation of equations and numerical solution

B.1. Case 1: Circumferential perturbations with constrained boundary

In order to perform efficient numerical computations, we define the dimensionless parameters

$$\rho = \frac{R}{B}, \quad \rho_1 = \frac{r}{B}, \quad f = \frac{\Delta f}{B}, \quad g = \Delta g, \qquad (B.1)$$

where B is the outer radius of constrained cylinder. On substitution of (B.1) in the governing Eqs. (3.6a) and (3.6b), we obtain the incremental differential equations in terms of dimensionless displacements f and g as

$$f'' = -\frac{1}{a_1}\left[a_2f' + a_3f + a_4g' + a_5g\right], \qquad (B.2)$$

$$g'' = -\frac{1}{b_1}\left[b_2g' + b_3g + b_4f' + b_5y_1\right], \qquad (B.3)$$

where

$$a_1 = \rho_1'\rho_1^2\rho^2\left[\alpha\rho_1'^2 - 2\log\left(\frac{\rho_1\rho_1'}{\rho}\right) + 2 + \alpha\right]f'',$$

$$a_2 = \rho_1\rho\left[[2\rho_1''\rho_1\rho - \rho_1'\rho_1]2\log\left(\frac{\rho_1\rho_1'}{\rho}\right) + \rho_1'^3\rho_1\alpha - 6\rho_1''\rho_1\rho - 2\rho_1''\rho_1\rho\alpha\right.$$
$$\left. - 2\rho_1'^2\rho + 4\rho_1'\rho_1 + \rho_1'\rho_1\alpha\right],$$

$$a_3 = \rho_1'\left[-\rho_1'^2\rho_1^2\alpha n^2 + \rho_1'^2\rho^2 2\log\left(\frac{\rho_1\rho_1'}{\rho}\right) - 2\rho_1''\rho_1\rho^2 - \rho_1'^2\rho_1^2\alpha - 4\rho_1'^2\rho^2\right.$$
$$\left. - \rho_1'^2\rho^2\alpha + 2\rho_1'\rho_1\rho\right],$$

$$a_4 = -\rho_1'^2\rho_1^2\rho^2 n\left[2\log\left(\frac{\rho_1\rho_1'}{\rho}\right) - 2 - \alpha\right],$$

$$a_5 = \rho_1'\rho_1 n\left[2\log\left(\frac{\rho_1\rho_1'}{\rho}\right)\rho_1'^2\rho^2 - 2\rho_1''\rho_1\rho^2 - \rho_1'^2\rho_1^2\alpha - 2\rho_1'^2\rho^2\right.$$
$$\left. - \rho_1'^2\rho^2\alpha + 2\rho_1'\rho_1\rho\right],$$

and

$$b_1 = \left[\rho_1'^2\rho_1^2\rho^2\alpha\right], \quad b_2 = -\rho_1'\rho_1\rho\left[-\rho_1'^2\rho\alpha + 2\log\left(\frac{\rho_1\rho_1'}{\rho}\right)\rho - \rho_1'\rho_1\alpha - \rho\alpha\right],$$

$$b_3 = \rho_1'^2 n^2\left[2\log\left(\frac{\rho_1\rho_1'}{\rho}\right)\rho^2 - \rho_1^2\alpha - 2\rho^2 - \rho^2\alpha\right],$$

$$b_4 = \rho_1'\rho^2 n\left[2\log\left(\frac{\rho_1\rho_1'}{\rho}\right) - 2 - \alpha\right],$$

$$b_5 = -n\left[[\rho_1''\rho^2 - \rho_1'\rho]2\log\left(\frac{\rho_1\rho_1'}{\rho}\right) - 2\rho_1''\rho^2 - \rho_1''\rho^2\alpha\right.$$
$$\left. + 2\rho_1'^2\rho_1\alpha + 2\rho_1'\rho + \rho_1'\rho\alpha\right],$$

subjected to non-dimensionalised boundary conditions at the inner surface of cylinder (at $\rho = A/B = A^*$)

$$[2\rho_1'A^*]f - \rho_1\left[-\rho_1'^2A^*\alpha + A^*\left[2\log\left(\frac{\rho_1\rho_1'}{A^*}\right)\right] + \rho_1\rho_1'\widetilde{P} - 2A^* \quad -A^*\alpha\right]f'$$
$$+ [2\rho_1\rho_1'A^*n]g = 0, \qquad (B.4a)$$

$$n\left[A^*\left[2\log\left(\frac{\rho_1\rho_1'}{A^*}\right)\right] + \rho_1\rho_1'\widetilde{P} - A^*\alpha\right]f + [A^*\rho_1^2\rho_1'\alpha]g' = 0, \qquad (B.4b)$$

where $\widetilde{P} = P_r/\kappa$ and $A^* = \rho|_{\mathrm{at}A/B}$. The constrained outer boundary at $\rho = 1$ leads to the condition

$$f(1) = g(1) = 0. \qquad (B.5)$$

B.2. Case 2: Circumferential perturbations with free boundary

In this case, the incremental ODEs is given by (B.2)–(B.3). The boundary conditions are obtained by using Eq. (3.4b) and the dimensionless parameters (B.1). The inner boundary, $\rho = A^*$ for free cylinder is given by

$$[2\rho_1'A^*]f - \rho_1\left[-\rho_1'^2A^*\alpha + A^*\left[2\log\left(\frac{\rho_1\rho_1'}{A^*}\right)\right] + \rho_1\rho_1'\widetilde{P} - 2A^* - A^*\alpha\right]f'$$
$$+ [2\rho_1\rho_1'A^*n]g = 0, \qquad (B.6a)$$

$$n\left[A^*\left[2\log\left(\frac{\rho_1\rho_1'}{A^*}\right)\right] + \rho_1\rho_1'\widetilde{P} - A^*\alpha\right]f + [A^*\rho_1^2\rho_1'\alpha]g' = 0, \qquad (B.6b)$$

and at the outer boundary, $\rho = 1$ is

$$[2\rho_1']f - \rho_1\left[-\rho_1'^2\alpha + \left[2\log\left(\frac{\rho_1\rho_1'}{1}\right)\right] - 2 - \alpha\right]f' + [2\rho_1\rho_1'n]g = 0, \qquad (B.7a)$$

$$n\left[\left[2\log\left(\frac{\rho_1\rho_1'}{1}\right)\right] - \alpha\right]f + [\rho_1^2\rho_1'\alpha]g' = 0. \qquad (B.7b)$$

B.3. Case 3: Axial perturbations with constrained boundary

We define the dimensionless parameters

$$\rho = \frac{R}{B}, \quad \rho_1 = \frac{r}{B}, \quad \bar{f} = \frac{\Delta\bar{f}}{B}, \quad \bar{h} = \frac{\Delta\bar{h}}{B}, \quad k = m\frac{2\pi}{L}B, \qquad (B.8)$$

that lead to reformulation of the governing Eqs. (3.9) as

$$\bar{f}'' = -\frac{1}{c_1^*}\left[c_2^*\bar{f}' + c_3^*\bar{f} + c_4^*\bar{h}' + c_5^*\bar{h}\right],$$
$$\bar{h}'' = -\frac{1}{d_1^*}\left[d_2^*\bar{h}' + d_3^*\bar{h} + d_4^*\bar{f}' + d_5^*\bar{f}\right], \qquad (B.9)$$

where the dimensionless coefficients are given by

$$c_1^* = \rho_1'\rho_1^2\rho^2\left[\rho_1'^2\alpha - 2\log\left(\frac{\rho_1\rho_1'}{\rho}\right) + 2 + \alpha\right],$$

$$c_2^* = \rho_1\rho\left[\rho_1'^3\rho_1\alpha + [2\rho_1\rho_1''\rho - \rho_1'\rho_1]\,2\log\left(\frac{\rho_1\rho_1'}{\rho}\right) - 2\rho_1'^2\rho - 6\rho_1\rho_1''\rho\right.$$
$$\left. - 2\rho_1\rho_1''\rho\alpha + 4\rho_1'\rho_1 + \rho_1'\rho_1\alpha\right],$$

$$c_3^* = -\rho_1'\left[\rho_1'^2\rho_1^2\rho^2\alpha k^2 - 2\log\left(\frac{\rho_1\rho_1'}{\rho}\right)\rho_1'^2\rho^2 + \rho_1'^2\rho_1^2\alpha + 4\rho_1'^2\rho^2 + \rho_1'^2\rho^2\alpha\right.$$

$$+ 2\rho_1 \rho_1'' \rho^2 - 2\rho_1' \rho_1 \rho\Big],$$

$$c_4^* = -\rho_1'^2 \rho_1^2 \rho^2 k \left[2 \log\left(\frac{\rho_1 \rho_1'}{\rho}\right) - 2 - \alpha\right],$$

$$c_5^* = -2\rho_1' \rho_1 \rho k \left[\rho_1'^2 \rho + \rho_1 \rho_1'' \rho - \rho_1' \rho_1\right],$$

$$d_1^* = \rho_1'^2 \rho \alpha, \qquad d_2^* = \rho_1'^2 \alpha, \qquad d_3^* = k^2 \rho \rho_1'^2 \left[2 \log\left(\frac{\rho_1 \rho_1'}{\rho}\right) - 2 - 2\alpha\right],$$

$$d_4^* = \rho_1' \rho k \left[2 \log\left(\frac{\rho_1 \rho_1'}{\rho}\right) - 2 - \alpha\right],$$

$$d_5^* = k \left[[\rho_1' - \rho_1'' \rho] \, 2 \log\left(\frac{\rho_1 \rho_1'}{\rho}\right) + 2\rho_1'' \rho + \rho_1'' \rho \alpha - 2\rho_1' - \rho_1' \alpha\right],$$

subjected to constrained boundary conditions

$$\left.\begin{array}{l} c_{11}^* \bar{f} + c_{22}^* \bar{f}' + c_{33}^* \bar{h} = 0, \\ d_{11}^* \bar{f} + d_{44}^* \bar{h}' = 0, \end{array}\right\} \qquad \text{at} \quad \rho = \frac{A}{B}, \tag{B.10a}$$

$$\bar{f}(1) = \bar{h}(1) = 0, \qquad \text{at} \qquad \rho = 1, \tag{B.10b}$$

and

$$c_{11}^* = 2\rho_1' A^*,$$

$$c_{22}^* = -\rho_1 \left[-\rho_1'^2 A^* \alpha + 2 \log\left(\frac{\rho_1 \rho_1'}{A^*}\right) A^* + \rho_1 \widetilde{P} \rho_1' - 2A^* - A^* \alpha\right],$$

$$c_{33}^* = 2\rho_1 \rho_1' A^* k,$$

$$d_{11}^* = k \left[2 \log\left(\frac{\rho_1 \rho_1'}{A^*}\right) A^* + \rho_1 \widetilde{P} \rho_1' - A^* \alpha\right], \qquad d_{44}^* = \alpha \rho_1' A^*,$$

here $A^* = \rho|_{\text{at} A/B}$.

B.4. Case 4: Axial perturbations with free boundary

The incremental differential equations for cylindrical channels with unconstrained boundary is same as (B.9) and the inner boundary ($\rho = A/B$) subjected to internal pressure is same as (B.10a). The boundary condition at the outer boundary at $\rho = 1$ is given by

$$[2\rho_1']\bar{f} - \rho_1 \left[-\rho_1'^2 \alpha + 2 \log\left(\rho_1 \rho_1'\right) A^* - 2 - \alpha\right]\bar{f}' + 2\rho_1 \rho_1' k\bar{h} = 0, \tag{B.11a}$$

$$k \left[2 \log\left(\rho_1 \rho_1'\right) - \alpha\right]\bar{f} + \alpha \rho_1' \bar{h}' = 0. \tag{B.11b}$$

B.5. Perturbation along radial component of cylinder for axial bifurcation

In this section, we discuss the special case for axial bifurcation where the radial component of cylinder is perturbed alone as discussed in Section 3.2. This type of perturbation result in second order incremental ODE which is obtained by setting the coefficients $c_4^* = c_5^* = d_1^* = d_2^* = d_3^* = d_4^* = d_5^* = 0$ in (B.9) and is given by

$$\rho_1' \rho_1^2 \rho^2 \left[\rho_1'^2 \alpha - 2 \log\left(\frac{\rho_1 \rho_1'}{\rho}\right) + 2 + \alpha\right]\widetilde{f}''$$

$$+ \rho_1 \rho \left[\rho_1'^3 \rho_1 \alpha + [2\rho_1 \rho_1'' \rho - \rho_1' \rho_1] \, 2 \log\left(\frac{\rho_1 \rho_1'}{\rho}\right) - 2\rho_1'^2 \rho - 6\rho_1 \rho_1'' \rho\right.$$

$$\left. - 2\rho_1 \rho_1'' \rho \alpha + 4\rho_1' \rho_1 + \rho_1' \rho_1 \alpha\right]\widetilde{f}' - \rho_1' \left[\rho_1'^2 \rho_1^2 \rho^2 \alpha \widetilde{k}^2 - 2 \log\left(\frac{\rho_1 \rho_1'}{\rho}\right)\rho_1'^2 \rho^2\right.$$

$$\left. + \rho_1'^2 \rho_1^2 \alpha + 4\rho_1'^2 \rho^2 + \rho_1'^2 \rho^2 \alpha + 2\rho_1 \rho_1'' \rho^2 - 2\rho_1' \rho_1 \rho\right]\widetilde{f} = 0, \tag{B.12}$$

where we use the non-dimensional parameter, $\widetilde{k} = \widetilde{m} 2\pi B/L$. Eq. (B.12) is subjected to internal pressure at inner boundary (at $\rho = A^*$) which is

given as

$$[2\rho_1' A^*]\widetilde{f} - \rho_1 \left[-\rho_1'^2 A^* \alpha + 2 \log\left(\frac{\rho_1 \rho_1'}{A^*}\right) A^* + \rho_1 \widetilde{P} \rho_1' - 2A^* - A^* \alpha\right]\widetilde{f}' = 0. \tag{B.13}$$

The boundary condition for the external constrained boundary (at $\rho = 1$) is

$$\widetilde{f}(1) = 0, \tag{B.14}$$

and for unconstrained external boundary is given by

$$[2\rho_1']\widetilde{f} - \rho_1 \left[-\rho_1'^2 \alpha + 2 \log\left(\rho_1 \rho_1'\right) - 2 - \alpha\right]\widetilde{f}' = 0. \tag{B.15}$$

Appendix C. Fibres in axial direction

The soft hyperelastic cylinder is made anisotropic by a reinforcement of fibres orientated along the vector **a**. To account for this reinforcement, the strain energy density function (2.4) has additional fibre terms as

$$\Omega^*(I_1, I_3, I_4) = \frac{\mu}{2}\left[I_1 - 3 - \log I_3\right] + \frac{\kappa}{4}\left[\log I_3\right]^2 + \Omega_f(I_4), \tag{C.1}$$

where $\Omega_f(I_4) = \frac{k_1}{2k_2}\left[\exp[k_2[I_4 - 1]^2] - 1\right]$ is the energy due to fibre reinforcement. The first Piola Kirchhoff stress corresponding to fibres reinforcement in axial direction is

$$\mathbf{P}_f = \frac{\partial \Omega_f}{\partial \mathbf{F}} = \frac{\partial \Omega_f}{\partial I_4}\frac{\partial I_4}{\partial \mathbf{F}} = \left[k_1[I_4 - 1]\exp[k_2[I_4 - 1]^2]\right]\left[2\mathbf{a} \otimes \mathbf{Fa}\right], \tag{C.2}$$

where **a** denote the unit vector which characterised the direction of fibres. The elastic moduli corresponding to fibre term is given by

$$\mathcal{A}^f = \frac{\partial \mathbf{P}_f}{\partial \mathbf{F}} = k_1 \left[\frac{\partial I_4}{\partial \mathbf{F}}\right]\exp[k_2[I_4 - 1]^2]\left[2\mathbf{a} \otimes \mathbf{Fa}\right] + k_1[I_4 - 1]$$

$$\times \frac{\partial}{\partial \mathbf{F}}\left[\exp[k_2[I_4 - 1]^2]\right]\left[2\mathbf{a} \otimes \mathbf{Fa}\right] + k_1[I_4 - 1]$$

$$\times \exp[k_2[I_4 - 1]^2]\frac{\partial}{\partial \mathbf{F}}\left(2\mathbf{a} \otimes \mathbf{Fa}\right), \tag{C.3}$$

which is written in index notation as

$$\mathcal{A}^f_{ijkl} = 2\left[k_1 \exp[k_2[I_4 - 1]^2]\left[[\mathbf{a} \otimes \mathbf{Fa}]_{ij}[\mathbf{a} \otimes \mathbf{Fa}]_{kl}\right]\right.$$

$$+ 2k_1[I_4 - 1]\exp[k_2[I_4 - 1]^2]2k_2[I_4 - 1]\left[[\mathbf{a} \otimes \mathbf{Fa}]_{ij}[\mathbf{a} \otimes \mathbf{Fa}]_{kl}\right]$$

$$\left. + 2k_1[I_4 - 1]\exp[k_2[I_4 - 1]^2]a_i a_j \delta_{kl}\right]. \tag{C.4}$$

Upon simplifying (C.4) we obtain

$$\mathcal{A}^f_{ijkl} = 2k_1 \exp[k_2[I_4 - 1]^2]\left[\left[1 + 2k_2[I_4 - 1]\right][\mathbf{a} \otimes \mathbf{Fa}]_{ij}[\mathbf{a} \otimes \mathbf{Fa}]_{kl}\right.$$

$$\left. + [I_4 - 1]a_i a_j \delta_{kl}\right]. \tag{C.5}$$

The incremental stress associated with the fibre term is

$$\delta \mathbf{P}_f = \mathcal{A}^f \delta \mathbf{F} = \mathcal{A}^f_{ijkl}[\delta \mathbf{F}]_{kl}. \tag{C.6}$$

This can be expanded by substituting (C.5) in (C.6) to get

$$\delta \mathbf{P}_f = 2k_1 \exp[k_2[I_4 - 1]^2]\left[1 + 2k_2[I_4 - 1]\right][\mathbf{a} \otimes \mathbf{Fa}]\left[\text{tr}\left(\delta \mathbf{F}^T[\mathbf{a} \otimes \mathbf{Fa}]\right)\right]$$

$$+ 2k_1[I_4 - 1]\exp[k_2[I_4 - 1]^2][\mathbf{a} \otimes \mathbf{a}]\text{tr}(\delta \mathbf{F}^T). \tag{C.7}$$

References

[1] B. Barrière, K. Sekimoto, L. Leibler, Peristaltic instability of cylindrical gels, J. Chem. Phys. 105 (4) (1996) 1735–1738.

[2] P. Ciarletta, M. Ben Amar, Peristaltic patterns for swelling and shrinking of soft cylindrical gels, Soft Matter 8 (6) (2012) 1760–1763.

[3] D.E. Moulton, A. Goriely, Circumferential buckling instability of a growing cylindrical tube, J. Mech. Phys. Solids 59 (3) (2011) 525–537.

[4] D.M. Haughton, R.W. Ogden, Bifurcation of inflated circular cylinders of elastic material under axial loading—I. Membrane theory for thin-walled tubes, J. Mech. Phys. Solids 27 (3) (1979) 179–212.

[5] R. Benedict, A. Wineman, W.H. Yang, The determination of limiting pressure in simultaneous elongation and inflation of nonlinear elastic tubes, Int. J. Solids Struct. 15 (3) (1979) 241–249.

[6] Y.B. Fu, S.P. Pearce, K.-K. Liu, Post-bifurcation analysis of a thin-walled hyperelastic tube under inflation, Int. J. Non-Linear Mech. 43 (8) (2008) 697–706.

[7] A. Dorfmann, D.M. Haughton, Stability and bifurcation of compressed elastic cylindrical tubes, Internat. J. Engrg. Sci. 44 (18–19) (2006) 1353–1365.

[8] H.-H. Dai, F.-F. Wang, Bifurcation to a corner-like formation in a slender nonlinearly elastic cylinder: Asymptotic solution and mechanism, Proc. R. Soc. Lond. Ser. A Math. Phys. Eng. Sci. 464 (2094) (2008) 1587–1613.

[9] H.-H. Dai, F.-F. Wang, J. Wang, J. Xu, Pitchfork and octopus bifurcations in a hyperelastic tube subjected to compression: Analytical post-bifurcation solutions and imperfection sensitivity, Math. Mech. Solids 20 (1) (2015) 25–52.

[10] Z.X. Cai, Y.B. Fu, Effects of pre-stretch, compressibility and material constitution on the period-doubling secondary bifurcation of a film/substrate bilayer, Int. J. Non-Linear Mech. 115 (2019) 11–19.

[11] A.D. Bakiler, B. Dortdivanlioglu, A. Javili, From beams to bilayers: A unifying approach towards instabilities of compressible domains under plane deformations, Int. J. Non-Linear Mech. 135 (2021) 103752.

[12] Y.-C. Chen, D.M. Haughton, Existence of exact solutions for the eversion of elastic cylinders, J. Elasticity 49 (1) (1997) 79–88.

[13] D.M. Haughton, Y.-C. Chen, Asymptotic bifurcation results for the eversion of elastic shells, Z. Angew. Math. Phys. ZAMP 54 (2) (2003) 191–211.

[14] S. Kyriakides, C. Yu-Chung, The initiation and propagation of a localized instability in an inflated elastic tube, Int. J. Solids Struct. 27 (9) (1991) 1085–1111.

[15] Y.B. Fu, J.L. Liu, G.S. Francisco, Localized bulging in an inflated cylindrical tube of arbitrary thickness–the effect of bending stiffness, J. Mech. Phys. Solids 90 (2016) 45–60.

[16] N. Cheewaruangroj, K. Leonavicius, S. Srinivas, J.S. Biggins, Peristaltic elastic instability in an inflated cylindrical channel, Phys. Rev. Lett. 122 (6) (2019) 068003.

[17] W. Hong, X. Zhao, Z. Suo, Formation of creases on the surfaces of elastomers and gels, Appl. Phys. Lett. 95 (11) (2009) 111901.

[18] E. Hohlfeld, L. Mahadevan, Unfolding the sulcus, Phys. Rev. Lett. 106 (10) (2011) 1–4, http://dx.doi.org/10.1103/PhysRevLett.106.105702, arXiv:1008.0694.

[19] T. Tallinen, J.S. Biggins, Mechanics of invagination and folding: Hybridized instabilities when one soft tissue grows on another, Phys. Rev. E 92 (2) (2015) 022720.

[20] S.S. Velankar, V. Lai, R.A. Vaia, Swelling-induced delamination causes folding of surface-tethered polymer gels, ACS Appl. Mater. Interfaces 4 (1) (2012) 24–29.

[21] A. Hasan, A. Paul, A. Memic, A. Khademhosseini, A multilayered microfluidic blood vessel-like structure, Biomed. Microdevices 17 (5) (2015) 1–13.

[22] D.M. Taghizadeh, A. Bagheri, H. Darijani, On the hyperelastic pressurized thick-walled spherical shells and cylindrical tubes using the analytical closed-form solutions, Int. J. Appl. Mech. 7 (02) (2015) 1550027.

[23] I.E. Araci, B. Su, S.R. Quake, Y. Mandel, An implantable microfluidic device for self-monitoring of intraocular pressure, Nature Med. 20 (9) (2014) 1074–1078.

[24] A. Koh, D. Kang, Y. Xue, S. Lee, R.M. Pielak, J. Kim, T. Hwang, S. Min, A. Banks, P. Bastien, et al., A soft, wearable microfluidic device for the capture, storage, and colorimetric sensing of sweat, Sci. Transl. Med. 8 (366) (2016) 366ra165.

[25] D. Rus, M.T. Tolley, Design, fabrication and control of soft robots, Nature 521 (7553) (2015) 467–475.

[26] C. Schumacher, B. Bickel, J. Rys, S. Marschner, C. Daraio, M. Gross, Microstructures to control elasticity in 3D printing, ACM Trans. Graph. 34 (4) (2015) 1–13.

[27] M.A. Unger, H.-P. Chou, T. Thorsen, A. Scherer, S.R. Quake, Monolithic microfabricated valves and pumps by multilayer soft lithography, Science 288 (5463) (2000) 113–116.

[28] J.-F. Louf, N.B. Lu, M.G. O'Connell, H.J. Cho, S.S. Datta, Under pressure: Hydrogel swelling in a granular medium, Sci. Adv. 7 (7) (2021) eabd2711.

[29] D.M. Haughton, R.W. Ogden, Bifurcation of inflated circular cylinders of elastic material under axial loading—II. Exact theory for thick-walled tubes, J. Mech. Phys. Solids 27 (5–6) (1979) 489–512.

[30] J. Sang, S. Xing, H. Liu, X. Li, J. Wang, Y. Lv, Large deformation analysis and stability analysis of a cylindrical rubber tube under internal pressure, J. Theoret. Appl. Mech. 55 (1) (2016) 177–188.

[31] Y. Liu, Axial and circumferential buckling of a hyperelastic tube under restricted compression, Int. J. Non-Linear Mech. 98 (2018) 145–153.

[32] Y. Anani, G. Rahimi, On the stability of internally pressurized thick-walled spherical and cylindrical shells made of functionally graded incompressible hyperelastic material, Lat. Am. J. Solids Struct. 15 (4) (2018).

[33] R.W. Ogden, Non-Linear Elastic Deformations, Courier Corporation, 1997.

[34] G. Limbert, E. Kuhl, On skin microrelief and the emergence of expression micro-wrinkles, Soft Matter 14 (8) (2018) 1292–1300.

[35] D.M. Haughton, R.W. Ogden, On the incremental equations in non-linear elasticity—II. Bifurcation of pressurized spherical shells, J. Mech. Phys. Solids 26 (2) (1978) 111–138.

[36] P. Saxena, Finite deformations and incremental axisymmetric motions of a magnetoelastic tube, Math. Mech. Solids 23 (6) (2018) 950–983.

[37] D.M. Haughton, A. Orr, On the eversion of compressible elastic cylinders, Int. J. Solids Struct. 34 (15) (1997) 1893–1914.

[38] D.M. Haughton, Evaluation of eigenfunctions from compound matrix variables in non-linear elasticity–I. Fourth order systems, J. Comput. Phys. 227 (9) (2008) 4478–4485.

[39] S. Mehta, G. Raju, P. Saxena, Growth induced instabilities in a circular hyperelastic plate, Int. J. Solids Struct. (2021) http://dx.doi.org/10.1016/j.ijsolstr.2021.03.013.

[40] J. D'Errico, Fminsearchbnd, fminsearchcon, 2021, MATLAB Central File Exchange https://www.mathworks.com/matlabcentral/fileexchange/8277-fminsearchbnd-fminsearchcon.

[41] G.A. Holzapfel, R.W. Ogden, Constitutive modelling of arteries, Proc. R. Soc. Lond. Ser. A Math. Phys. Eng. Sci. 466 (2118) (2010) 1551–1597.